JOURNAL OF SOLID STATE CHEMISTRY 108, 1–10 (1994)

β-$Cu_3Fe_4(VO_4)_6$: Structural Study and Relationships; Physical Properties

M. A. Lafontaine, J. M. Grenéche,* Y. Laligant, and G. Férey[1]

*Laboratoire des Fluorures, URA CNRS 449, *Equipe de Physique de l'Etat Condensé, URA CNRS 807, Faculté des Sciences, Université du Maine, Avenue O. Messiaen, 72017, Le Mans Cedex, France*

Received November 6, 1992; in revised form March 23, 1993; accepted March 25, 1993

A new form of $Cu_3Fe_4(VO_4)_6$, different from the mineral lyonsite, has been isolated. It is triclinic (S.G. $P\bar{1}$; a = 6.600(3) Å, b = 8.048(4) Å, c = 9.759(5) Å, α = 106.08(3)°, β = 103.72(3)°, γ = 102.28(2)°, V = 461.8 Å^3, Z = 1). This three dimensional compound is characterized by the existence of edge sharing octahedral dimers of iron, connected by VO_4 tetrahedra and two sorts of copper polyhedra: square planes and trigonal bipyramids. Some cationic disorder between octahedral iron and fivefold coordinated copper sites is, however, detected by Mössbauer spectroscopy. This structure is closely related to howardevansite $NaCuFe_2(VO_4)_3$ and to other phosphates, vanadates, and molybdates of various compositions which can however, be described in a common cell in order to explain the relationships among all these compounds. Finally, physical properties of this copper iron vanadate are given. $Cu_3Fe_4(VO_4)_6$ is a semiconductor ($E_a \sim 0.20$ eV). Below 15 K, it becomes antiferromagnetic.

INTRODUCTION

We have already described the crystal structure of mineral volborthite $Cu_3V_2O_7(OH)_2$, 2 H_2O and its structural evolution with temperature (1, 2, and refs. therein). The formation of anhydrous $Cu_3V_2O_8$ in its high pressure form (3) occurs between 280 and 325°C; it transforms at 560°C in the high temperature variety (4), identified by Hughes *et al.* (5), to the mineral mcbirneyite during his investigation of the minerals around Itzalco Volcano (El Salvador). Beside numerous copper vanadates, they also found and solved the structure of two vanadates containing both iron and copper: orthorhombic lyonsite $Cu_3Fe_4(VO_4)_6$ (6) (S.G. *Pmcn*, a = 10.296 Å, b = 17.207 Å, c = 4.910 Å) and triclinic howardevansite $NaCuFe_2(VO_4)_3$ (7) (S.G. $P\bar{1}$, a = 8.198 Å, b = 9.773 Å, c = 6.651 Å, α = 103.82°, β = 101.99°, γ = 106.74°). The synthetic homologues of these two minerals were of interest for their potential properties. If the synthesis of the latter gave the required compound, the former appeared with a different structure, whose X-ray powder pattern was curiously close to that of howardevansite, and this led us to examine this new form of $Cu_3Fe_4(VO_4)_6$.

The format of the paper is as follows: after the experimental section, the crystal structure of β-$Cu_3Fe_4(VO_4)_6$ will be presented. In a third part, the examination of the structural correlations between this new form, howardevansite, and some other vanadates, molybdates, or phosphates will explain that, despite different formula, all these compounds depend on the same polyhedral arrangement. Finally the electric and magnetic properties will be given, including Mössbauer results.

EXPERIMENTAL

The new form of $Cu_3Fe_4(VO_4)_6$ can be obtained as a black powder by heating at 750°C for 2 days stoichiometric mixtures of either $Cu_3V_2O_8$ and $FeVO_4$ (1 : 4) or the elementary oxides CuO, Fe_2O_3, and V_2O_5 (3 : 2 : 3). A longer heating (5 days), followed by slow cooling, gives very small crystals of medium quality, however, suitable for single crystal X-ray analysis.

The dimensions of the crystal used for the structural study were 0.05 × 0.04 × 0.03 mm. The details of the data collection on the diffractometer Siemens AED 2 are summarized in Table 1. The structure was solved using direct methods. The option TREF of the program SHELS 86 (8) gave the position of the metallic atoms, all considered in a first step with the diffusion factor of copper; their refinement (R = 0.27) followed by Fourier difference syntheses provided the location of all the oxygen atoms. Subsequent refinement of their position parameters and of isotropic thermal motions lowers R to 0.071. The examination of the crystal chemistry rather than of bond lengths then allows one to distinguish the nature of the different cations. Further refinements with the corresponding diffusion factors (9) and anisotropic thermal motion give R = 0.048 and R_w = 0.041. An attempt to refine the occupation factor of copper and iron on the corresponding sites, suggested by the following Mössbauer study did not improve significantly the results. Tables 2 and 3 provide the final

[1] To whom correspondence should be addressed.

0022-4596/94 $6.00

TABLE 1
Details of the X-Ray Data Collection of $Cu_3Fe_4(VO_4)_6$

Determination of cell parameters	22 reflections ($24° \leq 2\theta \leq 30°$)
Space group	$P\bar{1}$
Cell dimensions	$a = 6.600(3)$ Å $\quad \alpha = 106.08(3)°$
	$b = 8.048(4)$ Å $\quad \beta = 103.72(3)°$
	$c = 9.759(5)$ Å $\quad \gamma = 102.28(2)°$
	$V = 461.8$ Å^3 $\quad Z = 1$
Wavelength	0.71069 Å (Mo$K\alpha$)
Scan mode	ω—θ
Step scan	$38 \leq N \leq 42$, every 0.035° and 4 sec
Aperture	$D = 2.7$ mm
Absorption correction	Gaussian method
Transmission factors	$A_{max} = 0.766$; $A_{min} = 0.628$
Absorption coefficient	$\mu = 93.4$ cm^{-1}
Angular range of data collection	$2\theta \leq 60°$
Range of measured h, k, l	$-9 \leq h \leq 9$; $-11 \leq k \leq 11$; $0 \leq l \leq 13$
Standard reflections (3)	(0–34;)(−411); (−2–30)
Measured every	120 mn
Maximum intensity variation	5%
Measured reflections	2690
Independent ref. ($\|F\| > 6\sigma\|F\|$)	1339
Number of refined parameters	169
Secondary extinction factor	$1.8(2).10^{-7}$
Weighting scheme	$1.000/(\sigma^2(F) + 0.00021F^2)$
Final Fourier residuals	−1.36 to 1.37 e$^- \cdot$ Å^{-3}
R/R_w	0.048/0.041

TABLE 2
Atomic Coordinates, Isotropic Thermal Parameters, and Valence Bond Calculations (s) of β-$Cu_3Fe_4(VO_4)_6$

Atom	x/a	y/b	z/c	B(Å^2)[a]	s
Cu1	0	½	½	1.7(2)	1.76
Cu2	7226(3)	7085(2)	2093(2)	1.6(1)	2.12
Fe1	3805(3)	9487(3)	6078(2)	0.7(1)	2.99
Fe2	0410(3)	2035(3)	0091(2)	0.8(1)	3.11
V1	8917(3)	8998(3)	6644(3)	0.6(1)	4.90
V2	2208(3)	6546(2)	2699(3)	0.6(1)	5.21
V3	5903(3)	2681(2)	1236(2)	0.6(1)	5.18
O1	0778(13)	0591(11)	1444(10)	0.9(6)	2.02
O2	5611(14)	1363(12)	2296(10)	1.6(7)	2.04
O3	1765(14)	4381(11)	1833(10)	1.3(7)	2.35
O4	9960(14)	2843(12)	8319(10)	1.2(7)	1.98
O5	2396(14)	7842(13)	9721(11)	1.6(7)	2.05
O6	8715(14)	9775(11)	3506(11)	1.1(5)	2.09
O7	5267(14)	2340(12)	7345(11)	1.5(7)	1.98
O8	3417(14)	2373(11)	9889(10)	1.0(6)	1.93
O9	3314(14)	0362(12)	4267(10)	1.2(7)	1.96
O10	2077(14)	6913(11)	4518(10)	1.5(7)	2.25
O11	6996(15)	4854(13)	2432(12)	1.4(7)	1.99
O12	1301(14)	3131(12)	4202(10)	1.6(7)	2.49

Note. Atomic coordinates are multiplied by 10^4, and bond valence parameters (11), correspond to the expressions $\exp[(1.65 - R)/0.40]$ for Cu^{2+}, $0.5(2.012/R)^{5.3}$ for Fe^{3+} and $1.25(1.714/R)^{5.1}$ for V^{5+}.

[a] The list of U_{ij} can be obtained on request. The very large e.s.d. observed on B and U_{ij} values are due to the medium crystalline quality of the crystal.

positional and thermal parameters and the corresponding characteristic distances and angles in the structure respectively. A list of structure factors can be obtained on request to the authors.

Electric measurements were performed on pellets annealed at 600°C in air by the classical four-probe method in the temperature range 150–300 K. Magnetic susceptibility was measured between 4.2 and 300 K by the Faraday method. Transmission Mössbauer experiments were carried out over the same temperature range, using a spectrometer with a constant acceleration mode and with a ^{57}Co source diffused into a rhodium matrix. The spectra were recorded on powdered samples resulting from a mixture of β-$Cu_3Fe_4(VO_4)_6$ and of boron nitride, with 5 mg of iron per cm^2. Fit to the data were obtained with the program MOSFIT (10). The value of the temperature of magnetic order was deduced from the thermal evolution of the paramagnetic fraction (thermal scanning method).

DESCRIPTION OF THE STRUCTURE

The comparison between the densities of lyonsite (4.21 g $\cdot$ cm^{-3}) and of the title compound (3.97 g $\cdot$ cm^{-3}) shows that the former corresponds to the high pressure form of $Cu_3Fe_4(VO_4)_6$. Figures 1 and 2 give the projections of the structure along [100] and [010], respectively, and the coordination polyhedra for each cationic species: tetrahedron for V^{5+}, octahedron for Fe^{3+} and both trigonal bipyramid (Cu(2)) and square plane (Cu(1)) (rather than elongated octahedron) for Cu^{2+}. Indeed, for Cu(1), the two Cu–O(11) distances, close to 2.80 Å (i.e., the classical O–O distance), seem to be too long to really create a true bond. They correspond to less than 5% of the bond valence.

Fe(1) octahedra, and Fe(2) ones as well, form edge sharing dimeric clusters. However, their environment by VO_4 tetrahedra is different (Fig. 3). Around the Fe(2) cluster ($d_{Fe(2)-Fe(2)} = 3.095$ Å), ten VO_4 tetrahedra exist, sharing each one vertex with the Fe(2) dimer, and therefore create a $Fe(2)_2V_{10}$ entity. Only eight VO_4 tetrahedra are linked to the Fe(1) dimer ($d_{Fe(1)-Fe(1)} = 3.152$ Å), since two of them share two vertices, instead of one, with the dimer. They build up a $Fe(1)_2V_8$ unit.

VO_4 tetrahedra link the different dimers via their corners: $Fe(2)_2V_{10}$ units are linked to each other to build up sheets in the (**a**,**b**) plane, whereas $Fe(1)_2V_8$ ones form zigzag chains parallel to the **a** axis at $z = \frac{1}{2}$. VO_4 tetrahedra also ensure the connection between the planes at $z = 0$ and $z = \frac{1}{2}$. Such an arrangement creates two types of cavities: [100] tunnels, half occupied by Cu(1) ions with

TABLE 3

Characteristic Distances (Å) and Angles (°) in Copper, Iron and Vanadium Polyhedra in β-$Cu_3Fe_4(VO_4)_6$

Cu(1) polyhedron

Cu1	O12	O12	O10	O10	O11	O11
O12	*1.955(8)*	3.911(7)	2.892(12)	2.801(9)	3.695(8)	3.034(19)
O12	180.	*1.955(8)*	2.801(9)	2.892(12)	3.034(19)	3.695(8)
O10	91.8(6)	88.2(6)	*2.069(14)*	4.138(11)	3.266(13)	3.620(11)
O10	88.2(6)	91.8(6)	180	*2.069(14)*	3.620(11)	3.266(13)
O11	101.9(5)	78.1(8)	83.9(6)	96.1(6)	*2.758(14)*	3.516(20)
O11	78.1(8)	101.9(5)	96.1(6)	83.9(6)	180	*2.758(14)*

$\langle Cu(1)–O\rangle_{[4+2]}$ = 2.261 Å; $\langle Cu(1)–O\rangle_{[4]}$ = 2.012 Å.

Cu(2) trigonal bipyramid

Cu2	O11	O7	O4	O8	O6
O11	*1.896(17)*	2.549(10)	2.806(9)	3.559(4)	3.647(13)
O7	99.8(7)	*1.958(9)*	3.912(11)	3.012(11)	2.603(12)
O4	92.6(8)	165.9(6)	*1.984(10)*	2.593(10)	2.796(12)
O8	130.5(6)	96.9(7)	79.6(8)	*2.066(15)*	3.087(13)
O6	132.6(6)	80.0(8)	86.8(8)	96.0(7)	*2.086(5)*

$\langle Cu(2)–O\rangle$ = 1.998 Å.

Fe(1) octahedron

Fe1	O2	O6	O9	O9	O10	O7
O2	*1.886(11)*	2.833(8)	2.893(8)	3.943(9)	2.895(13)	3.046(12)
O6	94.5(6)	*1.972(10)*	3.906(11)	3.825(9)	3.053(11)	2.603(12)
O9	96.4(7)	160.2(6)	*1.993(10)*	3.616(10)	3.079(11)	2.784(13)
O9	176.6(6)	88.9(7)	80.4(8)	*2.059(11)*	2.818(12)	2.804(17)
O10	*93.6(8)*	*97.7(7)*	*98.1(7)*	*85.8(8)*	*2.082(7)*	4.217(8)
O7	97.6(7)	78.0(8)	84.2(8)	83.3(9)	168.3(4)	*2.157(8)*

$\langle Fe(1)–O\rangle$ = 2.025 Å.

Fe(2) octahedron

Fe2	O5	O4	O1	O8	O3	O1
O5	*1.924(9)*	2.830(8)	2.839(8)	3.917(13)	2.734(12)	2.943(10)
O4	92.6(7)	*1.991(16)*	3.946(6)	2.593(10)	3.130(12)	2.786(12)
O1	*92.9(7)*	*164.4(4)*	*1.993(16)*	*2.965(7)*	*2.876(12)*	*2.575(16)*
O8	169.4(6)	80.8(8)	95.6(6)	*2.009(10)*	2.726(11)	3.968(11)
O3	88.0(8)	103.0(7)	91.9(7)	85.4(8)	*2.009(10)*	4.070(4)
O1	94.6(7)	86.5(8)	78.5(9)	93.2(7)	170.1(4)	*2.076(4)*

$\langle Fe(2)–O\rangle$ = 2.000 Å.

V(1) tetrahedron

V1	O12	O6	O1	O9
O12	*1.641(9)*	2.673(11)	2.785(11)	2.834(11)
O6	105.2(8)	*1.724(9)*	2.826(8)	2.848(12)
O1	110.1(8)	108.6(8)	*1.756(10)*	2.941(12)
O9	111.7(7)	108.7(7)	112.4(8)	*1.783(9)*

$\langle V(1)–O\rangle$ = 1.726 Å.

V(2) tetrahedron

V2	O3	O7	O10	O4
O3	*1.585(9)*	2.707(11)	2.769(11)	2.738(10)
O7	106.8(8)	*1.733(10)*	2.900(8)	2.918(12)
O10	*109.9(8)*	*113.1(8)*	*1.743(10)*	2.856(12)
O4	105.3(7)	112.3(8)	108.3(8)	*1.781(10)*

$\langle V(2)–O\rangle$ = 1.711 Å.

V(3) tetrahedron

V3	O5	O2	O11	O8
O5	*1.670(12)*	2.753(8)	2.744(10)	2.748(12)
O2	110.2(6)	*1.688(6)*	2.719(14)	2.867(8)
O11	*109.2(7)*	*107.0(8)*	*1.696(15)*	*2.863(9)*
O8	106.3(7)	112.4(6)	111.8(7)	*1.762(8)*

$\langle V(3)–O\rangle$ = 1.704 Å.

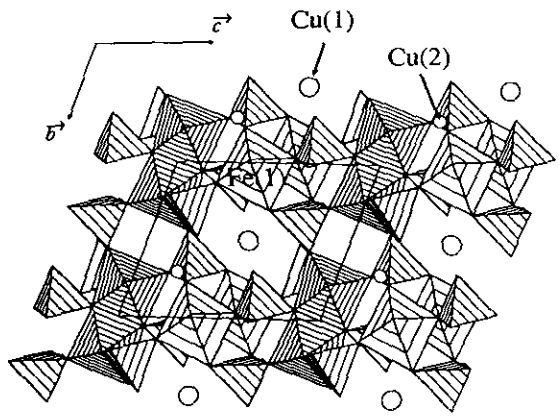

FIG. 1. (100) projection of β-$Cu_3Fe_4(VO_4)_6$; Strongly hatched octahedra correspond to Fe(2) which form files of dimers along [010]. Slightly hatched octahedra are Fe(1). Large circles are Cu(1) in 4 + 2 coordination; Cu(2) are represented by small circles.

$d_{Cu(1)-Cu(1)} = \mathbf{a} = 6.600$ Å within the tunnel, and also along this direction, sites containing fivefold coordinated Cu(2). This atom increases the cohesion between the two types of dimers since it shares its O(6)–O(7) edge with one Fe(1) octahedron, and its O(4)–O(8) edge with Fe(2) (Fig. 4). The occurrence and the occupancy of these cavities by several types of cations will be the object of the next part of the paper.

STRUCTURAL RELATIONSHIPS

β-$Cu_3Fe_4(VO_4)_6$ presents strong analogies with other phosphates, vanadates and molybdates previously described, whose formulae appear with the corresponding references in Table 4. Despite different formulations and, often, different cell parameters, they belong, as it will be shown below, to the same family to which can be ascribed to the general formula $A_xB_y(XO_4)_6$ ($A = Fe^{3+}$, Mg^{2+}, Cu^{2+}, Zn^{2+}, Co^{2+}, Na^+, and Ag^+; $B = Fe^{3+}$, Ti^{4+}, Mg^{2+}, Cu^{2+}, Zn^{2+}, Co^{2+}; $X = P^V$, V^V, Mo^{VI}, $6 \leq x + y \leq 8$). So, for a better comparison, we used the formalism previously described by Gicquel-Mayer and Mayer (12) to define a common cell, which is that of $ZnMoO_4$, to the different compounds. Table 4 contains the cell parameters published for the compounds, the new ones in the common cell and the corresponding transformation matrices. Using the common cell and a calculation of the new coordinates of the atoms in this cell, one then deduces the nature of the cations filling the different sites of the structure (Table 5). Whatever the compound may be, the sites corresponding to six- and fivefold coordinated cations are always occupied; site 3 (coordination 4 + 2) is filled if $x + y = 7$ (case of β-$Cu_3Fe_4(VO_4)_6$), whereas site 4 occupation (sevenfold coordination) relates to $x + y = 8$ (case of howardevansite $NaCuFe_2(VO_4)_3$). This latter remark obviously explains the so close similarity of the X-ray powder patterns of the two compounds.

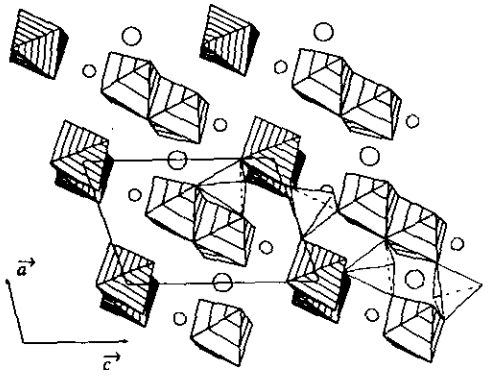

FIG. 2. (010) projection of β-$Cu_3Fe_4(VO_4)_6$; The same symbols as in Fig. 1 are used; for sake of clarity, only some vanadium tetrahedra are drawn.

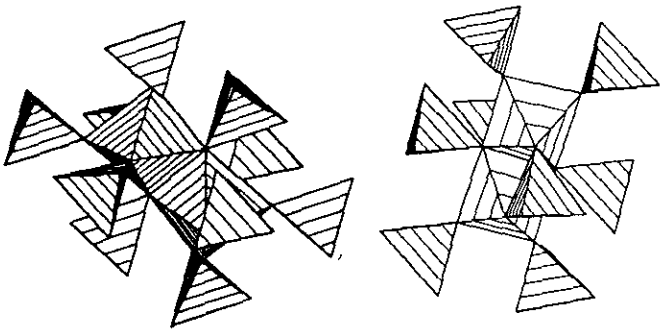

FIG. 3. Surrounding of the two types of dimers Fe(2) (left) and Fe(1) (right) by ten and eight vanadium tetrahedra respectively.

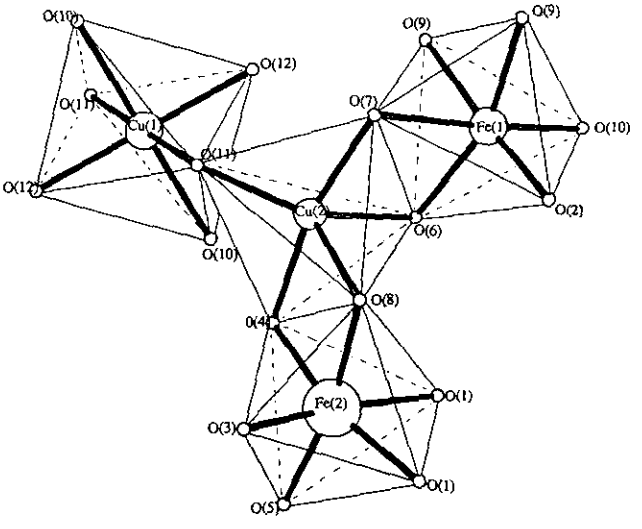

FIG. 4. Polyhedral arrangement around $Cu(2)O_5$ trigonal bipyramid.

TABLE 4
Cell Parameters of the Compounds Related to β-$Cu_3Fe_4(VO_4)_6$

Compound	Transf. Matrix[a]	a (Å) a' (Å)	b (Å) b' (Å)	c (Å) c' (Å)	α (°) α' (°)	β (°) β' (°)	γ (°) γ' (°)	V (Å^3)	Refs.
$ZnMoO_4$		9.625	6.965	8.373	103.28	96.30	106.72	514	12, 13
$FeVO_4$	1	6.719	8.060	9.254	96.65	106.57	101.60	465	14, 15
		9.254	*6.719*	*8.060*	*101.60*	*96.65*	*106.57*		
$Cu_3Fe_4(VO_4)_6$	4	6.600	8.048	9.759	106.08	103.72	102.28	461.8	this work
		9.560	*6.600*	*8.051*	*102.27*	*89.51*	*111.04*		
$Mg_3Ti_4(PO_4)_6$	2	6.931	7.962	9.430	67.61	69.35	79.33	414.0	16
		8.728	*6.931*	*7.962*	*100.67*	*92.55*	*107.25*		
$NaCuFe_2(VO_4)_3$	5	8.198	9.773	6.651	103.82	101.99	106.74	493.8	7
howardevansite		*9.544*	*6.651*	*8.198*	*101.99*	*89.41*	*111.29*		
$Ag_2Zn_2(MoO_4)_3$	2	6.992	8.712	10.818	64.24	66.51	76.27	543.0	12, 17
		9.749	*6.992*	*8.712*	*103.73*	*87.96*	*109.64*		
$Na_{0.5}Zn_{2.75}(MoO_4)_3$	2	6.983	8.594	10.825	65.87	66.19	78.17	542	12, 18
		9.879	*6.983*	*8.594*	*101.83*	*89.25*	*110.68*		
$NaZn_{2.5}(MoO_4)_3$	3	10.700	8.61	6.99	102.81	103.32	112.75	542	12, 18
		9.868	*6.99*	*8.61*	*102.81*	*89.02*	*110.27*		
$NaCo_{2.5}(MoO_4)_3$	3	10.590	8.64	6.98	103.46	102.66	112.24	540	12, 18
		9.807	*6.98*	*8.64*	*103.45*	*88.17*	*109.82*		
$NaMg_{2.5}(MoO_4)_3$	3	10.575	8.617	6.951	103.42	102.67	112.37	535	12, 19
		9.783	*6.951*	*8.617*	*103.42*	*88.33*	*109.83*		
$Na_{1.2}Mg_{2.4}(MoO_4)_3$	3	10.37	8.88	6.845	103.33	100.52	111.52	545	18, 19
		9.668	*6.845*	*8.880*	*103.33*	*86.22*	*107.56*		

Note. Values in italics correspond to the parameters after application of the transformation matrix.
[a] The different matrices defined by

$$\begin{bmatrix} a' \\ b' \\ c' \end{bmatrix} = M_n \cdot \begin{bmatrix} a \\ b \\ c \end{bmatrix} \quad \text{with } n\text{: } 1 \Rightarrow 5$$

are expressed as follows:

Matrix 1 $\begin{bmatrix} 0 & 1 & 0 \\ 0 & 0 & 1 \\ 1 & 0 & 0 \end{bmatrix}$ Matrix 2 $\begin{bmatrix} 0 & 1 & 0 \\ \frac{1}{2} & 0 & -1 \\ -1 & 0 & 0 \end{bmatrix}$ Matrix 3 $\begin{bmatrix} 1 & 0 & 0 \\ \frac{1}{2} & 0 & 1 \\ 0 & 1 & 0 \end{bmatrix}$ Matrix 4 $\begin{bmatrix} \frac{1}{2} & -1 & 0 \\ 1 & 0 & -1 \\ \frac{1}{2} & 0 & 0 \end{bmatrix}$ Matrix 5 $\begin{bmatrix} \frac{1}{2} & 0 & -1 \\ 1 & 0 & 0 \\ 1 & -1 & 0 \end{bmatrix}$

TABLE 5
Nature and Number of the Cations Occupying the Different Sites in the Common Cell of the Related Compounds

Compound	Site 1 (2*i*) Coordination 6	Site 2 (2*i*) Coordination 5	Site 3 (1*d*) Coordination 4 + 2	Site 4 (1*a*) Coordination 7
$ZnMoO_4$	2 × Zn	Zn	□	□
$FeVO_4$	2 × Fe	Fe	□	□
$Cu_3Fe_4(VO_4)_6$	Fe(1), Fe(2)	Cu(2)	Cu(1)	□
$Mg_3Ti_4(PO_4)_6$	[Ti,Mg(1)]	Mg	[Ti,Mg(1)]	□
$Na_{0.5}Zn_{2.75}(MoO_4)_3$	2 × Zn	0.75 Zn	Na	□
$NaZn_{2.5}(MoO_4)_3$	2 × Zn	0.5 Zn + 0.5 Na	Na	□
$NaCo_{2.5}(MoO_4)_3$	2 × Co	0.5 Co + 0.5 Na	Na	□
$NaMg_{2.5}(MoO_4)_3$	2 × Mg	0.5 Mg + 0.5 Na	Na	□
$NaCuFe_2(VO_4)_3$ Howardevansite	2 × Fe	Cu	Na	Na
$Ag_2Zn_2(MoO_4)_3$	2 × Zn	Ag	Ag	Ag

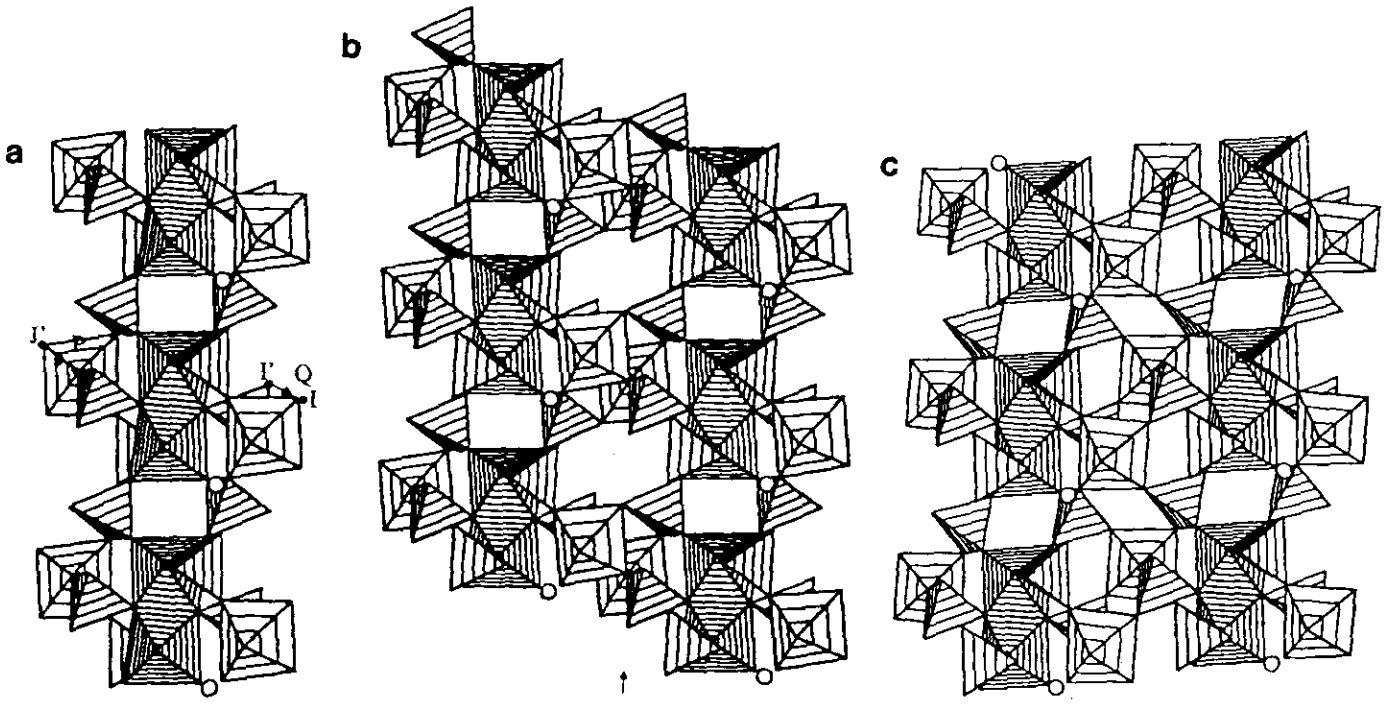

FIG. 5. (a) CBBU (see text) of the different structures. P and Q are the middles of JJ' and II' respectively. (b) Framework resulting from the application of the P operator; it corresponds to the title compound and howardevansite, with tunnels occupied by supplementary cations. (c) Framework of $FeVO_4$, obtained by the Q operation.

Another consequence of the above remark concerns the existence of a common basic building unit (CBBU) to all the compounds cited above. It is represented Fig. 5a, and formed by M_2X_{10} dimers (X = P, V, Mo) linked one to the other by two XO_4 tetrahedra in order to create infinite chains. The satellite octahedra, linked to $M_2^{\alpha}X_{10}$ dimers via XO_4 tetrahedra correspond to those which belong to $M_2^{\beta}X_8$ dimers in β-$Cu_3Fe_4(VO_4)_6$; the fivefold coordinated cations appear as circles in Fig. 5a. If one considers the positions of the symmetry centers of the common cell of the compounds cited above, they correspond to two different situations within the CBBU. The first is noted P (middle of an edge of M^{β} octahedron), and the second, Q (middle of the line II' joining the vertices of a satellite M^{β} octahedron and a tetrahedron). The P operator, applied to the CBBU, generates (Fig. 5b) the $M_2^{\beta}X_8$ dimers and the framework of the compounds of Table 5 except $ZnMoO_4$ and $FeVO_4$ which are formed if the Q operation arises (Fig. 5c). The tunnels, created by the P operation, can receive supplementary cations (sites 3 and 4 of Table 5). They are either half-filled, like in β-$Cu_3Fe_4(VO_4)_6$ (Cu1 in site 3) or filled like in howardevansite. The tunnels do not exist if Q is applied. Note that a simple shift between two CBBU of $ZnMoO_4$ gives the other structure.

PHYSICAL PROPERTIES

Electric Properties

Figures 6 and 7 show the thermal variation of the normalized resistance and the log σ vs $10^3/T$ plot respec-

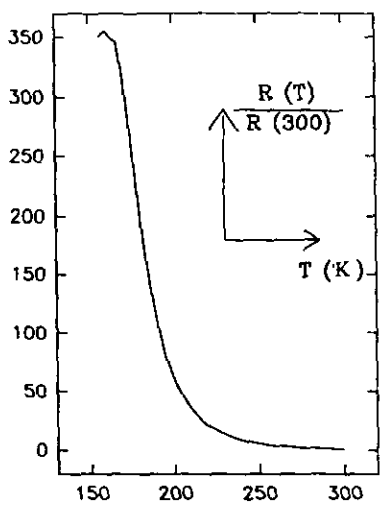

FIG. 6. Thermal evolution of $R(T)/R$ (300 K). [$R(300)$ = 75 Ω].

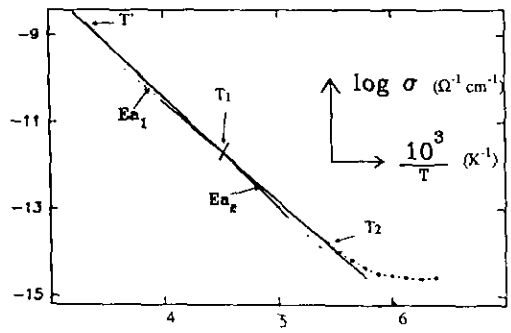

FIG. 7. Arrhenius plot of β-$Cu_3Fe_4(VO_4)_6$.

tively. They clearly indicate a semiconductor behavior with two domains 223 K $< T_1 <$ 300 K and $T_2 <$ 223 K, with two very close activation energies (E_{a1} = 0.22(1) eV and E_{a2} = 0.20(1) eV), corresponding to a very slight variation of the energy gap at 223 K, perhaps due to a structural transition.

Magnetic Properties

The simultaneous existence of magnetic dimers and of a triangular cationic topology around some sites incited us to explore the magnetic behaviour and eventual frustration effects in β-$Cu_3Fe_4(VO_4)_6$.

The inverse magnetic susceptibility (Fig. 8) varies linearly in the range 250–20 K. The experimental molar Curie constant (C_M = 19.0) is in good agreement with the theoretical value (C_{th} = 18.62). The negative value of θ_p (−80 K) indicates the presence of antiferromagnetic interactions. The antiferromagnetic ordering temperature value, estimated to 15 K from the accident observed on the $\chi^{-1}(T)$ curve, needed to be confirmed by Mössbauer spectroscopy.

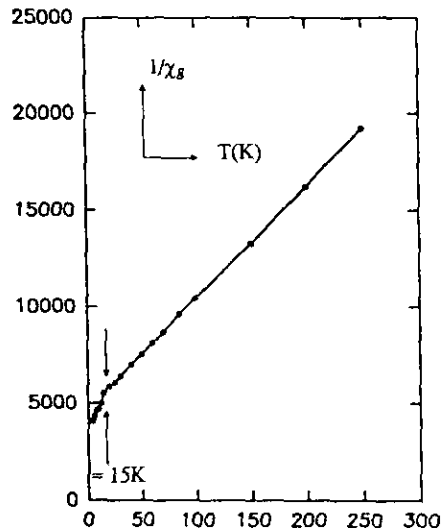

FIG. 8. Thermal variation of $\chi^{-1}(T)$.

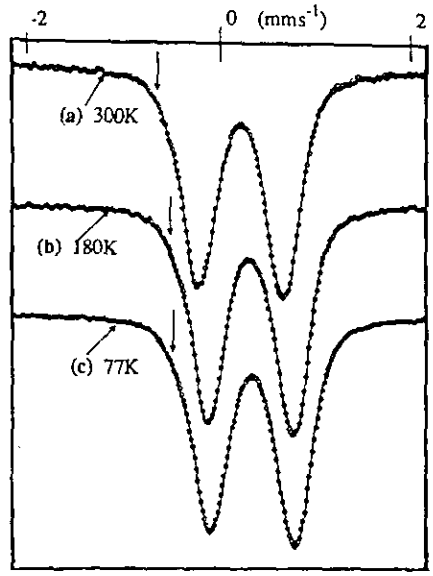

FIG. 9. Mössbauer spectra in the paramagnetic state; arrows indicate the shoulder leading to a third contribution.

Mössbauer Measurements

The spectra recorded at 300, 180, and 77 K (Fig. 9a–9c), indicate the presence of pure electric hyperfine interactions. These paramagnetic spectra exhibit a weak asymmetry. At every temperature, the fitting of these spectra by considering only two contributions was not sufficient to take into account the shoulder on the left line. An additional contribution was introduced in the fitting procedure. It provides good qualities of fit, whatever the hypothesis done for the two main contributions, considered either independent or equiprobable. Table 6 gathers the corresponding refined values.

The main comments on these results are the following (i) the narrow lines indicate the good crystallinity of the compound, (ii) the isomer shift values of sites 1 and 2 give evidence for sixfold coordinated trivalent iron ions, in agreement with the previous crystallographic data, (iii) the quadrupole splitting values of the sites 1 and 3 are very close, and (iv) the smaller isomer shift value of the third component reveals a lower coordination for iron. Consequently, it can be concluded to the occurrence of a partial cationic inversion between Fe^{3+} and Cu^{2+} (<10%). Crystal chemistry considerations (no known example of iron in square plane coordination) and comparison with Mössbauer data of fivefold coordinated Fe^{3+} (20, 21) lead one to conclude that the inversion exclusively occurs be-

TABLE 6
Refined Mössbauer Parameters in the Paramagnetic State

	T (K)								
	300			180			77		
Contributions[a]	1	2	3	1	2	3	1	2	3
I.S. ($mm \cdot s^{-1}$)	**0.40**	**0.38**	**0.25**	**0.47**	**0.46**	**0.31**	**0.51**	**0.50**	**0.35**
	0.39	*0.38*	*0.25*	*0.46*	*0.46*	*0.37*	*0.50*	*0.49*	*0.36*
Γ ($mm \cdot s^{-1}$)	**0.29**	**0.31**	**0.25**	**0.28**	**0.31**	**0.24**	**0.29**	**0.29**	**0.26**
	0.30	*0.30*	*0.28*	*0.30*	*0.30*	*0.21*	*0.30*	*0.30*	*0.25*
Q.S. ($mm \cdot s^{-1}$)	**1.01**	**0.69**	**1.14**	**1.01**	**0.70**	**1.14**	**0.97**	**0.65**	**1.09**
	1.02	*0.71*	*1.15*	*1.01*	*0.73*	*1.29*	*1.01*	*0.72*	*1.15*
Prop. (%)	**49**	**43**	**8**	**50**	**42**	**8**	**59**	**31**	**10**
	46	*46*	*8*	*47*	*47*	*6*	*46*	*46*	*8*

Note. Bold numbers correspond to the hypothesis of independent contributions and italics to equiprobable contributions. I.S.: Isomer shift ($mm \cdot s^{-1}$) with reference to metallic iron at 300 K (e.s.d. 0.02). Γ: Linewidth at half height ($mm \cdot s^{-1}$) of the lorentzian peak (e.s.d. 0.02). Q.S.: Quadrupolar splitting ($mm \cdot s^{-1}$) (e.s.d. 0.02). Prop.: Relative intensity (%) of the contribution (e.s.d. 3).

[a] Contributions 1 and 2 correspond to those of Fe^{3+} in octahedral coordination, and contribution 3 to fivefold coordinated Fe^{3+} contribution.

tween the octahedra and the trigonal bipyramid mainly occupied by Cu(2).

Below T_N, the Mössbauer spectra, collected at 1.8, 4.2, and 10 K (Fig. 10), confirm the existence of a three dimensional magnetic order. At 1.8 and 4.2 K, the sextets are well resolved, but the lines exhibit inhomogeneous broadenings. These broadenings can be attributed to either a non magnetically saturated state (even at 1.8 K) or a distribution of hyperfine fields in which the Fermi term results from the various surroundings of the Fe^{3+} nuclei, due to the local cationic disorder. Consequently, the refinement of these spectra requires a discrete distribution of hyperfine fields, to account for the line broadening. In the present study, the spectra were well reproduced by considering at least five different contributions (Table 7). Four of them, correspond to the high values of both hyper-

TABLE 7
Refined Mössbauer Parameters in the Magnetic State

T (K)	I.S. ($mm \cdot s^{-1}$)	Γ ($mm \cdot s^{-1}$)	2ε ($mm \cdot s^{-1}$)	H_{hf} (kOe)	Prop. (%)
1.8 K	0.50	0.48	−0.26	498	23
	0.50	0.48	−0.34	485	23
	0.51	0.48	−0.29	474	23
	0.51	0.48	−0.20	452	23
	0.36	0.48	−0.09	417	8
4.2 K	0.50	0.51	−0.28	480	23
	0.50	0.51	−0.37	466	23
	0.51	0.51	−0.28	450	23
	0.51	0.51	−0.26	417	23
	0.36	0.44	−0.20	364	8
10 K	0.54	0.90	−0.41	416	22
	0.54	0.90	−0.41	368	22
	0.54	0.90	−0.41	305	22
	0.54	0.90	−0.41	216	22
	0.35	0.60	−0.20	119	6 (6% para)

Note. I.S.: Isomer shift ($mm \cdot s^{-1}$) with reference to metallic iron at 300 K (e.s.d. 0.02). Γ: Linewidth at half height ($mm \cdot s^{-1}$) of the lorentzian peak (e.s.d. 0.05). 2ε: Quadrupolar shift ($mm \cdot s^{-1}$) (e.s.d. 0.05). H_{hf}: Hyperfine field (kOe); (e.s.d. 5 at 1.8 K and 4.2 K and 20 at 10 K). Prop.: Relative intensity (%) of the contribution (e.s.d. 5).

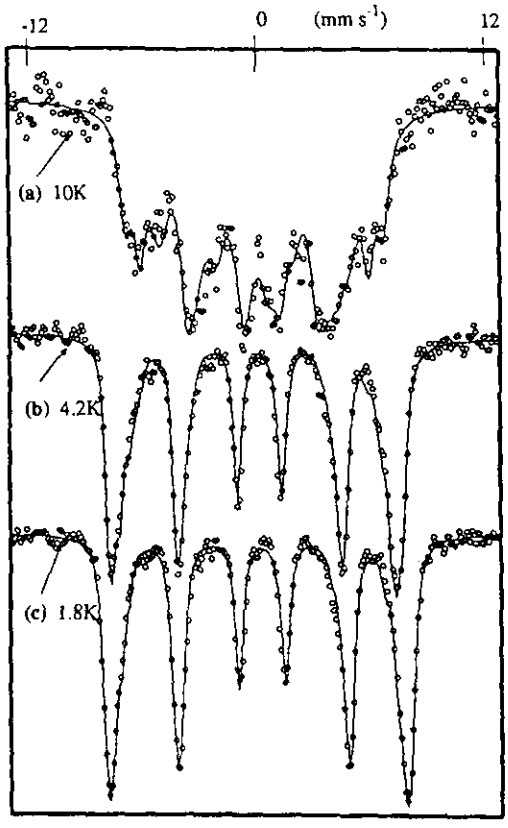

FIG. 10. Mössbauer spectra in the magnetic state.

fine field and isomer shift, and can be associated with Fe^{3+} in octahedral coordination; the last probably reflects fivefold coordinated iron(III). These results confirm the cationic inversion already mentioned.

The thermal evolution of the hyperfine field (Fig. 11) illustrates the disparity of behavior of the different contributions, leading to an eventual dispersion of the ordering temperatures, which could explain the rather large (3 K) temperature range observed for the occurrence of the magnetic order (Fig. 12). These results may be correlated with both the existence of isolated clusters in the structure

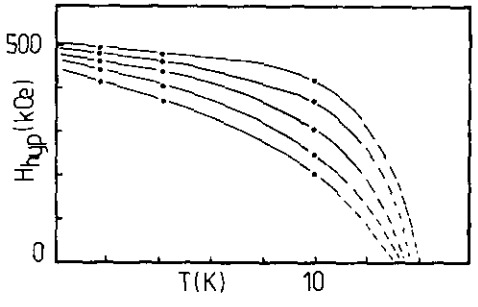

FIG. 11. Thermal variation of the hyperfine fields; line is only a guide for the eye.

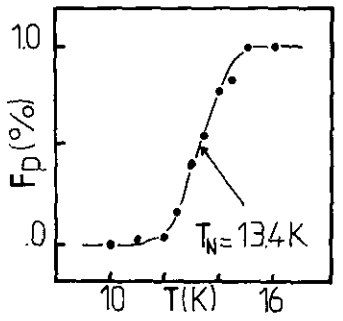

FIG. 12. Thermal evolution of the paramagnetic fraction (T = 13.4 K for R = 0.5).

and of cationic disorder on the metallic subnetwork. One cannot, however, rule out the presence of a small amount of impurity whose magnetic ordering temperature should be close to that of β-$Cu_3Fe_4(VO_4)_6$.

Neutron Diffraction

Diffraction patterns were collected on the D1B diffractometer at ILL at 80 and 1.9 K. Unfortunately, the difference pattern does not show any significant magnetic contribution to the diffraction, except for the (100) peak which had a noticeable intensity. It was not therefore possible to go further in our magnetic study, and describe the magnetic structure of this compound.

CONCLUSION

We have isolated a new form of β-$Cu_3Fe_4(VO_4)_6$ and described its structure close to howardevansite. Relationships with other phosphates and molybdates have been established, and the physical properties of electric semiconduction and of antiferromagnetism below 15 K have been described. Another compound exists in the pseudobinary system $Cu_3V_2O_8$–$FeVO_4$: its study is currently in progress.

ACKNOWLEDGMENTS

The authors are very indebted to Pr M. Leblanc (Université du Maine) for the collection of X ray data. The valuable comments of Dr Le Bail have been appreciated.

REFERENCES

1. M. A. Lafontaine, A. Le Bail, and G. Férey, *J. Solid State Chem.* **85,** 220 (1990).
2. M. A. Lafontaine, J. Rodriguez, and G. Férey, *Eur. J. Solid State Inorg. Chem.* **27,** 771 (1990).
3. R. D. Shannon, and C. Calvo, *Can. J. Chem.* **48,** 890 (1970).
4. J. Coing-Boyat, *Acta Crystallogr. Sect. B* **38,** 1546 (1982).
5. J. M. Hughes, B. S. Christian, L. W. Finger, and L. L. Malinconico, *J. Volc. Geoth. Res.* **33,** 183 (1987).

6. J. M. Hughes, S. J. Starkey, M. L. Malinconico, and L. L. Malinconico, *Am. Mineral.* **72,** 1000 (1987).
7. J. M. Hughes, J. W. Drexler, C. F. Campana, and M. L. Malinconico, *Am. Mineral.* **73,** 181 (1988).
8. G. M. Sheldrick "SHELS86" *in* "Crystallographic Computing" (G. M. Sheldrick, C. Kruger, and R. Goddard, Eds.), p. 175. Oxford Univ. Press, London/New York, 1985.
9. "International Tables of Crystallography" (Th. Hahn, Ed.). Norwell, MA, Kluwer, 1987.
10. J. Teillet, J. M., Greneche, and F. Varret, Mosfit Program (unpublished).
11. I. D. Brown and R. D. Shannon, *Acta Crystallogr. Sect. A* **29,** 266 (1973).
12. C. Gicquel-Mayer and M. Mayer, *Rev. Chim. Miner.* **20,** 88 (1983).
13. S. C. Abrahams, *J. Chem. Phys.* **46**(6), 2052 (1987).
14. B. Robertson and E. Kostiner, *J. Solid State Chem.* **4,** 29 (1972).
15. J. Muller and J. C. Joubert, *J. Solid State Chem.* **14,** 8 (1975).
16. A. Benmoussa, M. M. Borel, A. Grandin, A. Leclaire, and B. Raveau, *J. Solid State Chem.* **84,** 299 (1990).
17. C. Gicquel-Mayer, M. Mayer, and G. Perez, *Acta Crystallogr. Sect. B* **37,** 1035 (1981).
18. R. F. Klevtsova, V. G. Khim, and P. V. Klevtsov, *Kristallografiya* **25,** 1148 (1980).
19. V. A. Efremon, V. M. Zhukouski'i, and Y. G. Petrosyan, *Russ. J. Inorg. Chem.* **21**(1), 112 (1976).
20. J. Emery, A. Cereze, and F. Varret, *J. Phys. Chem. Solids* **41,** 1036 (1980).
21. J. Pannetier and P. Batail, *J. Solid State Chem.* **39,** 15 (1981).